

## Room evacuation in the presence of obstacles using an agent-based model with turning behavior

Yu Bao

School of Civil Engineering and Architecture, Wuhan University of Technology, China



### ARTICLE INFO

**Keywords:**

Agent-based model  
Evacuation  
Obstacle  
Route choice  
Rotation

### ABSTRACT

Pedestrian evacuation in a room environment is critical to architectural design, safety management and code development. The complexity of this issue is further increased in the presence of multiple obstacles, which may affect pedestrian dynamics and evacuation pattern. Most of previous studies on the room evacuation in the presence of multiple obstacles do not account for pedestrian's turning or rotational behavior, this paper aims to address this limitation. For this purpose, a previously developed agent-based model considering agent's turning behavior is extended in the context of room evacuation. Several improvements are made to this model, including: a procedure for generating feasible evacuation routes based on concepts of visible regions and accessible nodes; a deterministic approach based on the estimated evacuation time to select final evacuation route from feasible ones; and reformulation of agent's attractive potential to consider its movement along evacuation route. Simulation results with the proposed agent-based model are compared with published experimental data, and reasonable agreement can be observed. It is concluded that the proposed agent-based model is suitable for studying room evacuation problem in the presence of multiple obstacles under relatively low density scenario.

### 1. Introduction

Understanding pedestrian dynamics in room evacuation is an essential and critical part for risk management and development of safety protocol under various natural hazards, such as when fire occurs in a high-rise building [1] or an earthquake hits a large-scale city region [2]. The most distinct feature associated with room evacuation is the presence of multiple obstacles (e.g. table, chair and bookcase etc.). These obstacles will affect the choice of evacuation route and agent's behavior, thus pedestrian dynamics may exhibit a complex pattern given different configurations of obstacles. Consequently, the route choice has become a central theme for many studies related to room evacuation. The route choice behavior can either be formulated with a continuous space representation (e.g. Hoogendoorn and Bovy [3]; Asano et al. [4]) or a discrete space representation (e.g. Lo et al. [5]; Varas et al. [6]; Huang and Guo [7]; Alizadeh [8]; Guo and Huang [9]; Haghani and Sarvi [10]; Lovreglio et al. [11]; Choi and Chi [12]). In the discrete space representation, a pedestrian selects an exit based on its potential value or floor field (Kirchner and Schadschneider [13]). This scalar quantity considers pedestrian's distance to the exit, the congestion level and evacuation capacity of the exit in a comprehensive way. Thus it becomes very popular within the research community. Besides these numerical simulations, there have been considerable efforts to conduct experimental studies on this complex route choice issue. Liao et al. [14] used an experiment involving nearly 140 volunteers to investigate how the decision of initial route choice was made and how this decision could be revised during evacuation process.

E-mail address: [bao.yu@whut.edu.cn](mailto:bao.yu@whut.edu.cn).

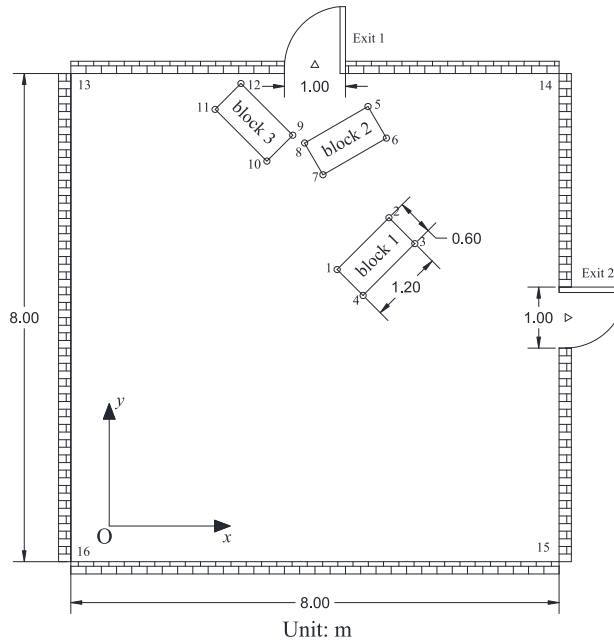


**Fig. 1.** Sample room configuration with multiple exits and obstacles.

Haghani et al. [15] experimentally studied the evacuation behavior under normal and high level of urgency, in particular, they investigated three major factors: reaction time, exit choice and exit-choice adaption. Li et al. [16] combined field study and virtual experiment to study effect of distance to exit, walking speed along routes and pedestrian density on the route choice behavior.

The route choice behavior must be implemented simultaneously with the pedestrian evacuation process. Pedestrian evacuation is primarily investigated using numerical methods due to efficiency, reliability and ethics reason. Similar to the classification of route choice behavior, pedestrian evacuation can be conducted in a continuous or discrete manner. The most popular continuous formulation is the Social Force Model (SFM), which is originally developed by Helbing and Molnar [17]. It has been successfully applied in various room evacuation scenarios, such as: Frank and Dorso [18] used SFM to study the effect of different shapes of obstacles on the evacuation time; Jia et al. [19] developed a SFM considering evading and surpassing behavior in the evacuation process; Xie et al. [20] considered the group effect in the SFM and found it was beneficial towards the overall crowd evacuation; Zhang et al. [21] used a two-layer SFM to investigate the total evacuation time under earthquake emergency. Discrete formulation of pedestrian evacuation includes cellular automaton (CA) model and agent-based model. CA model requires pre-defined grids so pedestrian can choose to occupy one of them during movement. For example, Zhu et al. [22] proposed a modified CA to study the crowd evacuation in a room with multiple obstacles considering effect of aisles; Yuan and Tan [23] developed a CA model with findings of tenability analysis in the evacuation problem; Pereira et al. [24] adopted a new CA model incorporating route changes and group effects; Lu et al. [25] studied the crowd evacuation using an extended CA model including the leader-follower behavior. Agent-based model, on the other hand, does not require these grids for locomotion, thus offering a more flexible framework compared to CA. It also has a wide application in a variety of evacuation scenarios (e.g. Chooramun et al. [26]; Kim and Han [27]; Ha and Lykotrafitis [28]; Turner and Penn [29]). While the majority of studies on the pedestrian evacuation focus on numerical aspect, there are also some experimental investigations. Zuriguela et al. [30] conducted an experiment to investigate the obstacle effect in a highly competitive evacuation process; Garcimartín et al. [31] performed a similar experimental investigation. Both of these experimental studies suggest placing an obstacle near the exit may not be beneficial towards overall crowd evacuation process. This is contradictory to other experimental results (e.g. Zhao et al. [32]), which suggest obstacle is beneficial. This highlights the complexity of role of obstacle in the crowd evacuation.

Pedestrian's turning or rotational behavior is relatively less addressed in the past studies. From our daily experience, pedestrian's moving ability is clearly affected by its facing direction. Existing experimental results (e.g. Yamamoto et al. [33]; Jin et al. [34]) also suggest the turning behavior of pedestrian may be critical to understanding certain phenomena in the evacuation process. Motivated from this observation, several studies have attempted to integrate this behavior, most of which are based on CA model. Miyagawa and Ichinose [35] studied turning behavior in CA model with each pedestrian occupying two adjacent cells, and their study found turning behavior was beneficial in terms of reducing evacuation time. Fu et al. [36] developed a finer discrete field CA model to account for pedestrian's turning behavior. Further, based on this model, Fu et al. [37] investigated how fatigue affected the overall evacuation performance. Integrating turning behavior into CA model may suffer from some limitations, the most notable one is that pedestrian's rotational angle is limited to  $\pm 45^\circ$  or  $\pm 90^\circ$ , depending on the neighborhood condition. Recently Bao and Huo [38] proposed an agent-based model incorporating rotational behavior to overcome the limitation with CA model. This agent-based model, however, is specifically designed for staircase evacuation.

This study aims to extend the agent-based model with turning behavior by Bao and Huo [38] to the room evacuation problem. To

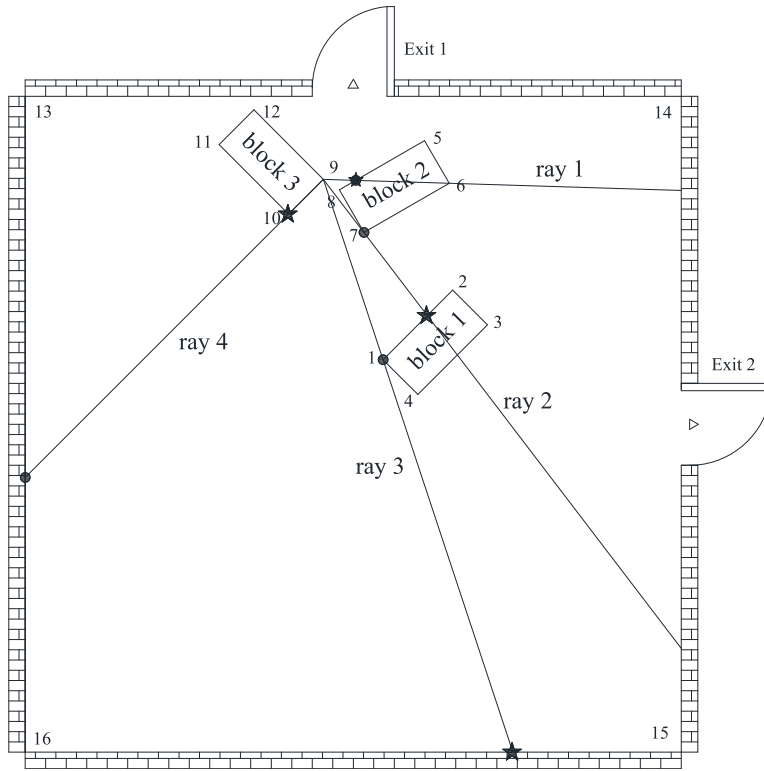


**Fig. 2.** Illustration of sight rays and polygon nodes (on clockwise and counter-clockwise side) using node 9 as an example.

this end, several improvements are made to the original agent-based model in [38], including: the development of visible region, accessible and inaccessible node, as well as feasible evacuation routes; a deterministic approach based on the estimated evacuation time to determine each agent's final evacuation route; and reformulation of the attractive potential to account for the characteristic of movement along its final evacuation route. Simulation results with the proposed agent-based model indicate it can reproduce experimental results with reasonable accuracy, thus validating its effectiveness. The rest of this paper is organized as follows: Section 2 describes the concept of visible region for a node or an exit, accessible and inaccessible nodes, and how to utilize these concepts to generate feasible evacuation routes with a specific room configuration; Section 3 discusses the deterministic approach based on the estimated evacuation time to select the final evacuation route from feasible ones. Subsequently, the attractive potential of an agent is reformulated to consider its movement along the selected evacuation route; Section 4 presents the simulation results with the proposed agent-based model and comparisons with published experimental data; Section 5 concludes the whole study.

## 2. Planning of evacuation route

During room evacuation in the presence of multiple obstacles, an agent must select a route based on a comprehensive consideration, including but not limited to: the location of possible exits, travelling time to different exits and how to bypass obstacles that may encounter. Thus evacuation route planning is the most important issue for the successful application of subsequent agent-based modeling. This section describes how an agent plans its evacuation route given a sample room configuration. In this paper, obstacle is represented by a rectangular shape (or a block), which is an idealization of many non-structural components that can be found in a built environment.

For a clear and concrete illustration of the development of the whole modeling procedure in this study, a simple room with two exits shown in Fig. 1 is used as an example even though no simulation is performed with respect to it. The two exits are numbered as 1 and 2, respectively. The length and width of the room are both 8 m. Each exit has a width of 1 m and its center coincides with wall. There are three obstacles in the room (referred to as block hereafter), their locations and rotation angles are selected such that this specific configuration can cover as many issues that may encounter during modeling as possible and these blocks do not overlap with each other. Please note this study focuses on configuration of practical value. Extreme configuration, such as obstacle locating at corners, falls outside the scope. Every node of the block is assigned a number for the ease of presentation, and the two nodes associated with each wall are also numbered, as depicted in Fig. 1. Let the bottom left corner be the origin of a Cartesian coordinate system, and counter-clockwise rotation be positive. The centroid  $C_i$  and rotation angle of each block  $\theta_i$  are given as ( $i = 1, 2, 3$ ):  $C_1 = [5, 5]$ ,  $\theta_1 = \pi/4$ ,  $C_2 = [4.5, 6.9]$ ,  $\theta_2 = \pi/6$ ,  $C_3 = [3, 7.2]$ ,  $\theta_3 = 3\pi/4$ .

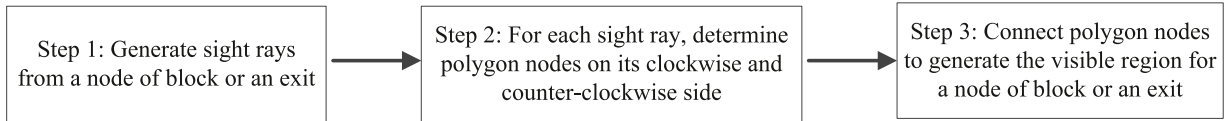


**Fig. 3.** General procedure for constructing a visible region.

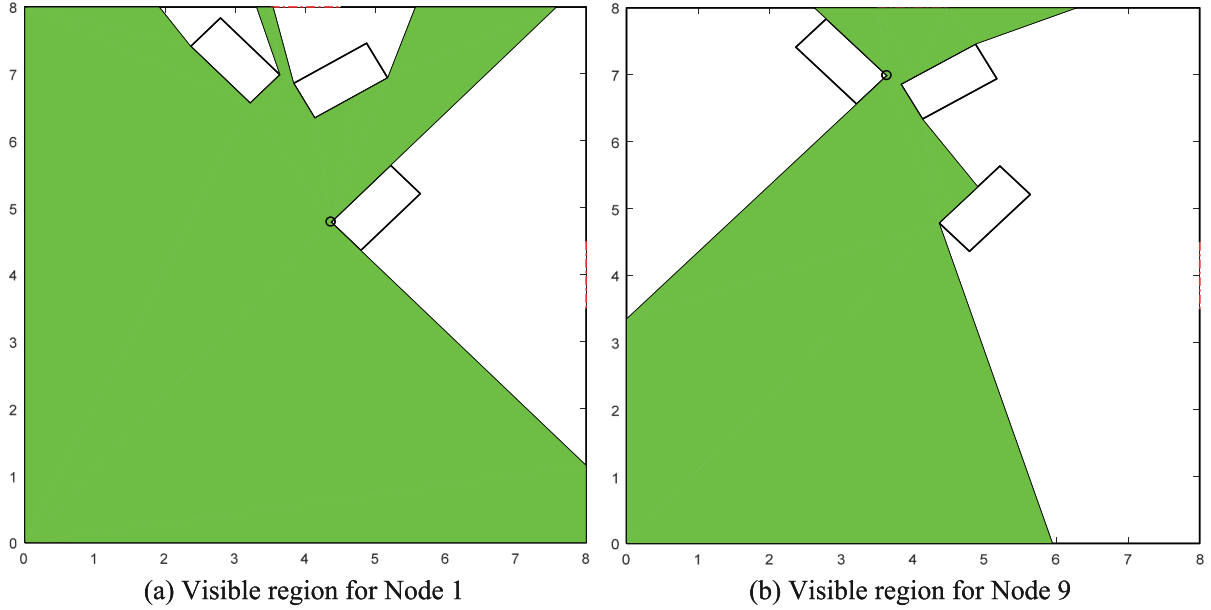


**Fig. 4.** Visible region generated for two sample nodes.

## 2.1. Visible region for node and exit

The central aspect of evacuation path planning is generating the visible region for each node of the block and exit. A visible region for a node is defined as a polygon within which agent can see this node without being obstructed. A similar definition can be made for an exit. It is clear that visible region for a node or an exit is only dependent on the topological relations between blocks and exits within a room, thus it can be determined as a priori before the agent-based simulation, which is a great advantage because it significantly improves numerical efficiency.

Before describing how to generate a visible region for a particular node or exit, it is useful to clarify several sets of concepts, which will be frequently used in the subsequent paragraphs. The first set of concepts is *partial obstruction* and *full obstruction* for a sight ray. When a sight ray intersects with a block only through one of its nodes or one of its edges, this is referred to as a *partial obstruction*, otherwise it is a *full obstruction*. The second set of concepts is the *clockwise side* and *counter-clockwise side* of a sight ray. These concepts are quite self-explanatory. Using the sight rays originating from node 9 as an example, as shown in Fig. 2, it can be seen that sight ray 1 is fully obstructed by block 2. Sight ray 2 is fully obstructed by block 1 but only partially obstructed by block 2. In addition, for sight ray 2, the partial obstruction of block 2 lies on the counter-clockwise side; similarly, the partial obstruction of block 3 for sight ray 4 is on the clockwise side. Note that we cannot distinguish which side it is on for the case of full obstruction.

There are three general steps to generate a visible region for a node of block or an exit, as shown in Fig. 3. The first step is to connect the node or exit, for which the visible region is developed, to all remaining nodes in the room, including those associated with blocks and walls. In the sample room configuration in Fig. 1, for each node of any block there are fifteen sight rays (for an exit there are sixteen), which includes eleven connecting remaining nodes of three blocks and four nodes of walls. Four sample sight rays originating from node 9 are illustrated in Fig. 2.

The second step is to determine the two polygon nodes locating on clockwise and counter-clockwise side of each sight ray. Since the room is an enclosed area, each sight ray is guaranteed to have an intersection point with a wall. Along the sight ray to this intersection point on the wall, it may intersect with multiple blocks. For each intersected block, it is necessary to determine whether it is a full or a partial obstruction; if it is a partial obstruction, which side of sight ray is located needs to be further determined; the coordinates of all intersection points need to be computed as well. After this, the polygon node on the clockwise side of each sight ray can be determined using the following procedure: the intersection point on the wall, those associated with full obstruction, as well as those with partial obstruction on the clockwise side are grouped together and sorted based on their relative Euclidean distance to the original node. Note

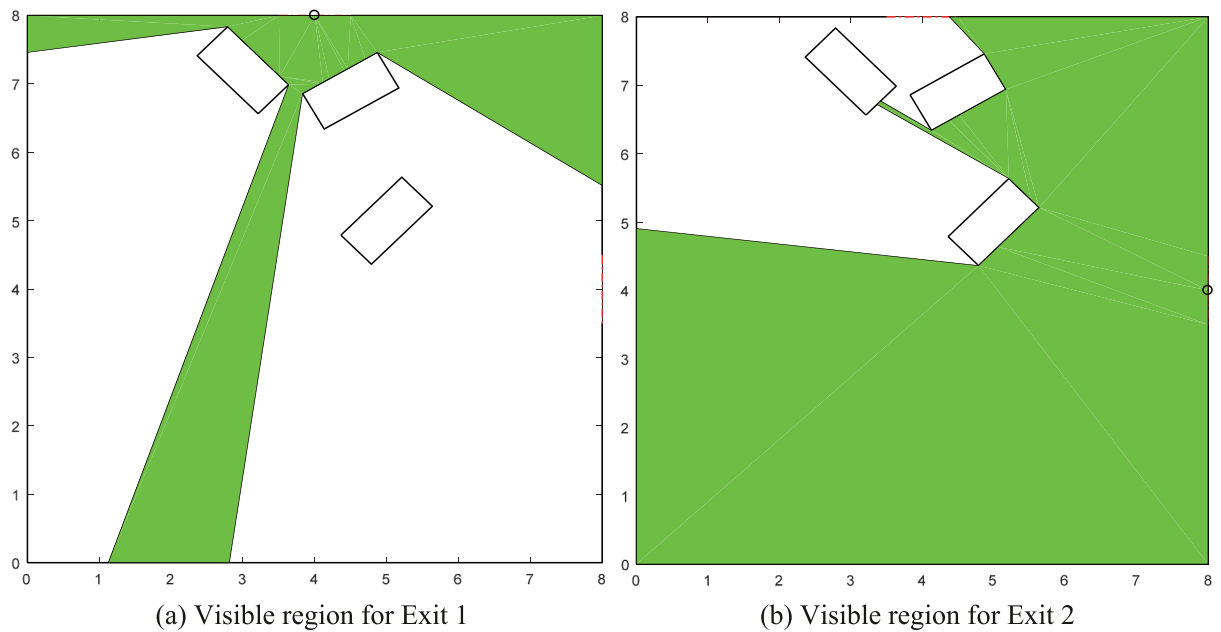


**Fig. 5.** Visible region generated for two exits.

that the original node of the sight ray is not included for this sorting process except for the case that the sight ray is in full obstruction with the block to which the originating node belongs. The purpose of this process is to exclude the area contained by the block in the visible region. The intersection point with the minimal relative distance is the polygon node on the clockwise side. The procedure to identify the polygon node on the counter-clockwise side of a sight ray is identical. The two polygon nodes for each sample sight ray are also shown in Fig. 2. The solid circular symbol indicates the polygon node on the counter-clockwise side of the sight ray, while the solid star symbol indicates the other side. Note that for sight ray 1 these two polygon nodes coincide.

The third step is to connect the identified polygon nodes to form visible region. For this purpose, the order of each sight ray needs to be determined at first. In this study, the relative rotation angle of each sight ray with respect to the horizontal  $x$  axis is first computed, assuming counter-clockwise rotation is positive and it lies within the interval from zero to  $2\pi$ . Based on the rotation angle of each sight, they can be arranged in an ascending order to form a sorted list of sight rays. After this sorting process, the visible polygon can be generated by connecting the following two polygon nodes on two consecutive sight rays on the list: one on the counter-clockwise side of the sight ray with relatively smaller rotation angle, and the other on the clockwise side of the sight ray with relatively larger one. The only exception to this rule is for the first and last sight ray located on the sorting list. In this case, polygon node on the counter-clockwise side is associated with relatively larger rotation angle, which is in contrast to the previous description. It is not hard to see that if there are  $n$  sight rays on the sorted list, the above process repeats  $n$  times. The visible regions for node 1 and 9 using the above method are presented as shaded area in Fig. 4. The same procedure can be also applied to generate a visible region for an exit, which is shown in Fig. 5. In both figures, the circular symbol indicates where the node or exit center locates.

## 2.2. Accessible and inaccessible nodes

In this study, the nodes of every block are used as basis for generating feasible evacuation paths. However, not all nodes can be used because some of them may be so close to adjacent wall or another node that an agent cannot pass through. In light of this observation, it is necessary to identify which node can be accessed by agent during planning of evacuation path, and it is referred to as *accessible node* in this study. Conversely, when a node is too close to an adjacent wall or another node, it is classified as *inaccessible node*. The procedure to identify the accessible nodes, as well as construct the so-called '*obstructed line*', is presented in Fig. 6. In this procedure, the minimal distance of a node to a wall means: (1) if the projection point of this node locates within the line segment of the wall, it is the projection distance; (2) otherwise it is the smaller value of distances from this node to each node of the wall. This is identical to the definition used in [38]. The quantity  $l_t$  is a threshold value below which agent is unable to pass through. Using the room configuration shown Fig. 1 as an example and assuming a threshold value  $l_t = 0.4$  m throughout this study (which equals to the diameter of torso of an agent, as depicted in Fig. 10(b)), the accessible and inaccessible nodes, as well as the obstructed lines can be identified in Fig. 7. In this figure the accessible nodes are indicated with a circular symbol while the inaccessible ones are shown with triangular symbol. In addition, the obstructed line, which connects either two inaccessible nodes or one inaccessible node and its projection point on a wall, is illustrated with a solid line.

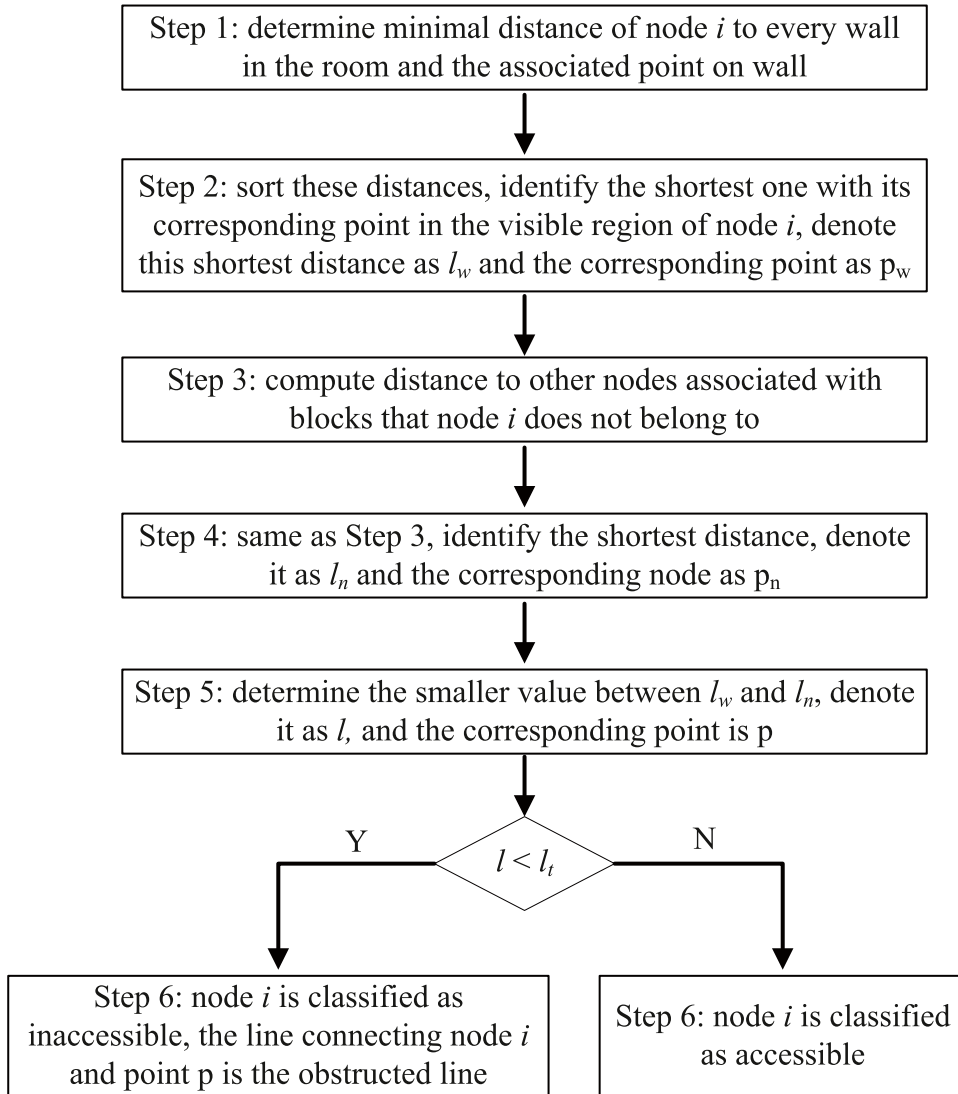


**Fig. 6.** Procedure to classify sample node  $i$  as accessible or inaccessible.

### 2.3. Feasible evacuation routes

With all accessible nodes and obstructed lines identified, next step is to generate feasible evacuation routes for an agent to travel to a certain exit. The feasible evacuation routes in this study are represented by a multi-level multi-node tree structure. Between two adjacent levels, one node at the top level is connected to one or multiple nodes at the bottom level, which forms a parent-child relation. Because this tree structure comprehensively considers the topological relation among the accessible nodes, obstructed lines and exit, it becomes the cornerstone for room evacuation problem. The general procedure to generate feasible evacuation routes given an exit is presented in Fig. 8. Several observations can be made regarding this procedure: (1) it heavily relies on the visible region for a node or an exit; (2) the development of visible region does not account for the presence of obstructed lines, therefore evacuation routes that intersect with obstructed lines are explicitly handled; (3) it is a greedy algorithm since only all accessible nodes are included in the feasible evacuation routes, but not all possible evacuation routes. This is a reasonable choice because an exhaustive evaluation of evacuation routes is extremely cumbersome even for a relatively simple room configuration.

The sample room configuration in Fig. 1 is again used as an example to illustrate the above procedure. The feasible evacuation routes for two exits are presented in Fig. 9. Using exit 1 as an example, it can be seen that the feasible evacuation routes are represented by a five-level tree structure with number of every accessible node indicated inside a circle. Between two consecutive levels, node at the top level (i.e. level with a smaller number) is the parent node and nodes at the bottom level are the child ones. For each parent node, there may be multiple child nodes directly connecting it. The actual evacuation route for an agent can be directly obtained from the feasible evacuation routes using a bottom-up searching approach: given any accessible node number, locate its position in the tree

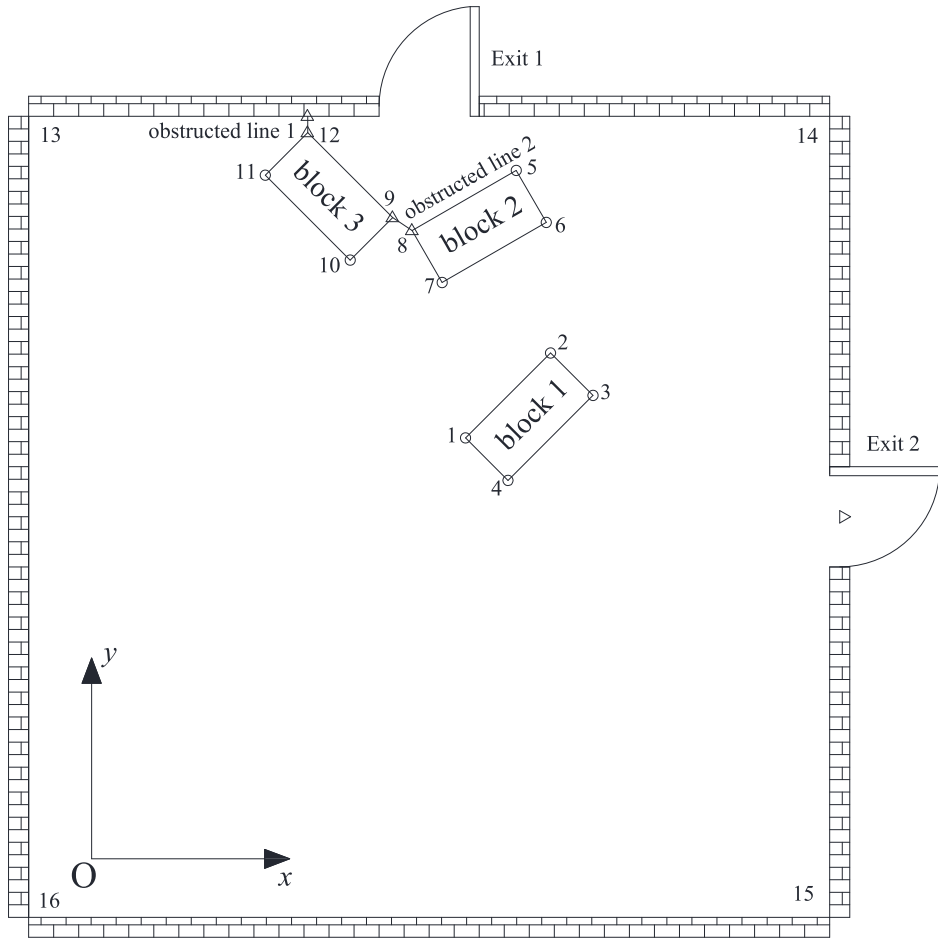


**Fig. 7.** Accessible, inaccessible nodes and obstructed lines in the sample room.

structure, keep searching for its parent node until the first level (i.e. an exit) is reached. The choice of final evacuation route from feasible ones is further described in the following section.

### 3. Agent-based modeling with rotational behavior

The framework of agent-based modeling with rotational behavior in this study is adopted from Bao and Huo [38], and it is briefly covered here for the completeness of this study. Each agent has three degrees-of-freedom (i.e. DOF): two translational ( $x$  and  $y$ ) and one rotational DOF ( $\theta$ ), as shown in Fig. 10(a). The translational DOF is measured with respect to the global coordinate  $xoy$  and rotational DOF is related to the angle between global and co-rotational coordinate  $x'y'$ . An agent is represented by a circle with a radius of  $R_t = 0.2$  m unless otherwise stated. The dashed elliptic shape in Fig. 10(b) denotes agent's physical boundary that cannot be overlapped, which is characterized by minor and major axis length  $R_x$  and  $R_y$ . An agent has forward translational and angular velocity, they are denoted as  $v_f$  and  $\omega$  respectively. The lateral and backward translation velocity, denoted as  $v_l$  and  $v_b$ , are assumed to have the following deterministic relations with  $v_f$ :  $v_b = v_f/3$ ,  $v_l = v_f/2$ . In this framework, given a finite time step, agent first performs rotational behavior, followed by its translational behavior. Note that rotational behavior may not occupy the whole discrete time step so translational behavior can still happen. These behaviors are guided by minimizing its total potential, which consists of attractive and repulsive potential. The former potential reflects agent's desire to achieve a certain goal, and the latter one represents agent's interaction with surrounding built environment and other agents. To improve numerical efficiency, both translational and rotational behaviors are discretized. In Fig. 10(c) and (d) the trial directions and positions are illustrated, where  $\Delta\theta = \omega * \Delta t$ ,  $d_{forward} = v_f * \Delta t$ ,  $d_{lateral} = v_l * \Delta t$ ,  $d_{backward} = v_b * \Delta t$  and  $\Delta t$  is the time increment for agent-based simulation. For more detailed descriptions regarding this framework, readers are referred to [38]. This section does not aim to provide a comprehensive description of this agent-based model, but to offer key improvements in the context of room evacuation in the presence of multiple obstacles. Specifically, the choice of final evacuation route and the reformulation of attractive are presented in detail.

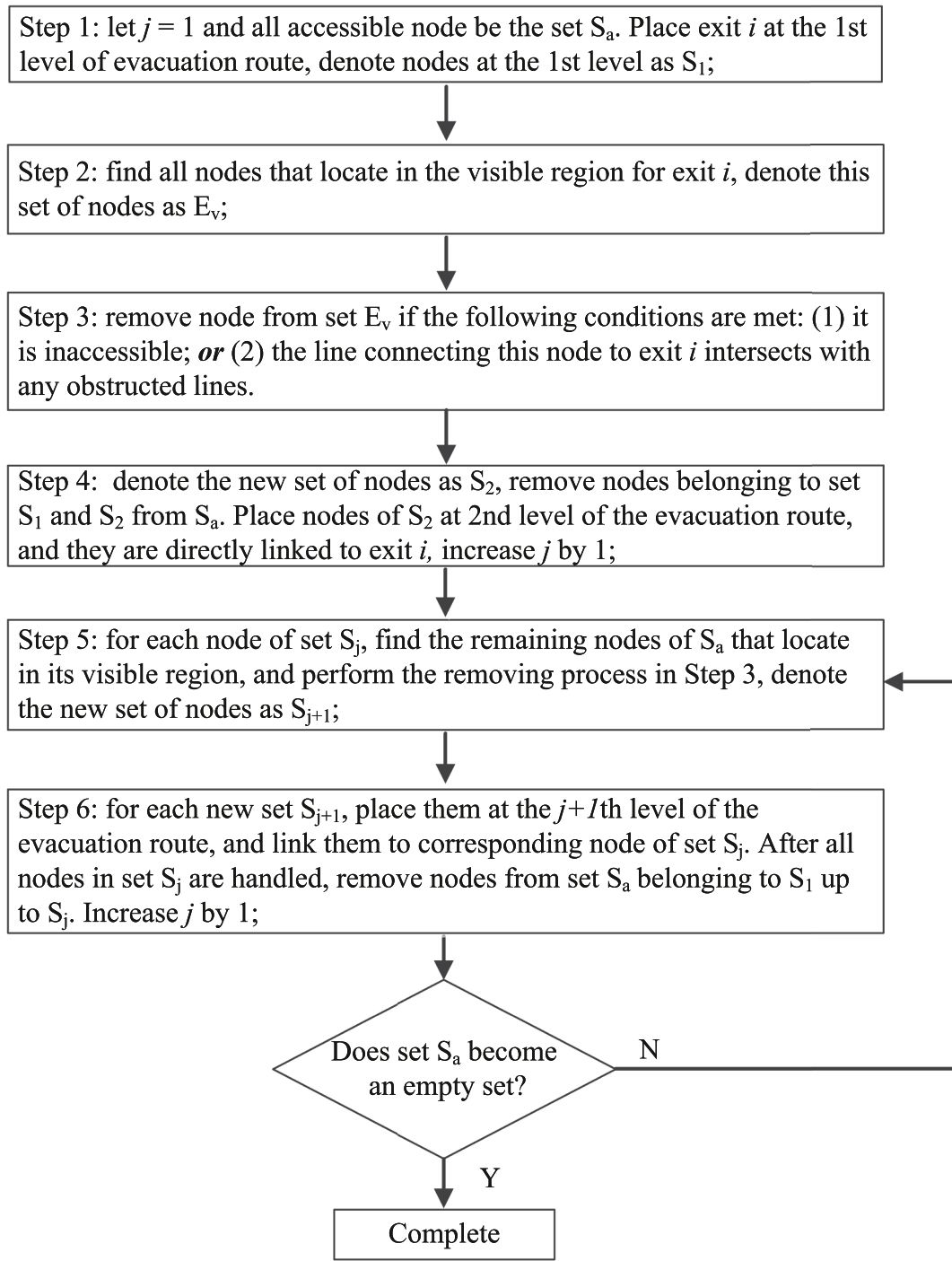


**Fig. 8.** Procedure to determine the feasible evacuation routes given an exit.

### 3.1. Choice of final evacuation route

In this study, the feasible evacuation routes are geometrically represented by polylines connecting an exit, multiple accessible nodes and agent's current position. One important task with the room evacuation is the choice of final evacuation route from feasible ones. It is assumed that agent cannot directly pass but can see through an obstacle. Agent's sight is represented by a series of rectangular shapes (termed as sight blocks hereafter) distributing along each feasible evacuation route. For the ease of presentation, one

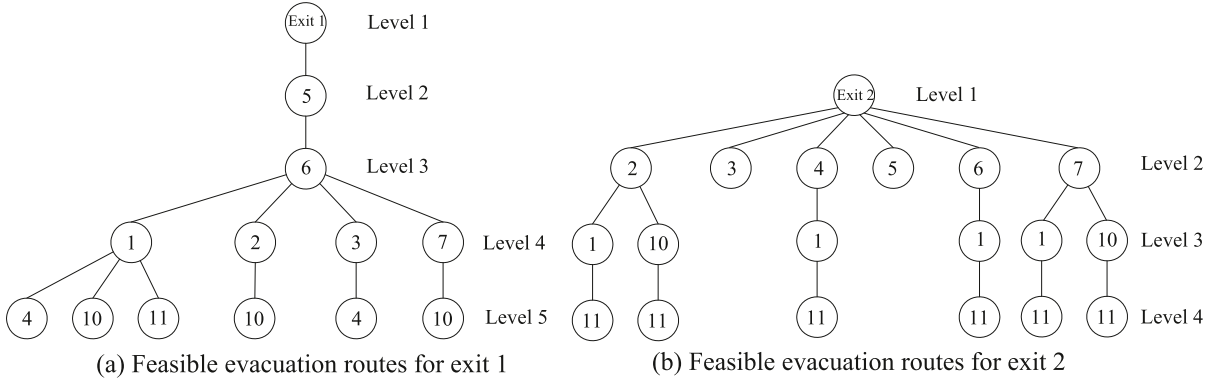


Fig. 9. Feasible evacuation routes represented by a tree-structure for two exits in the sample room.

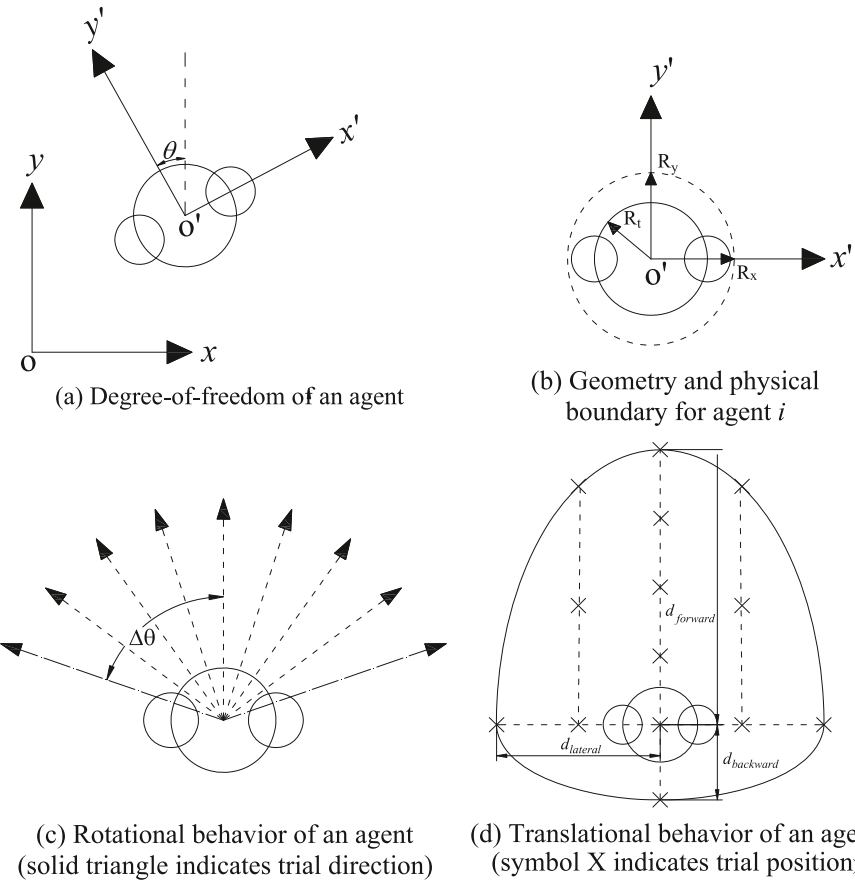
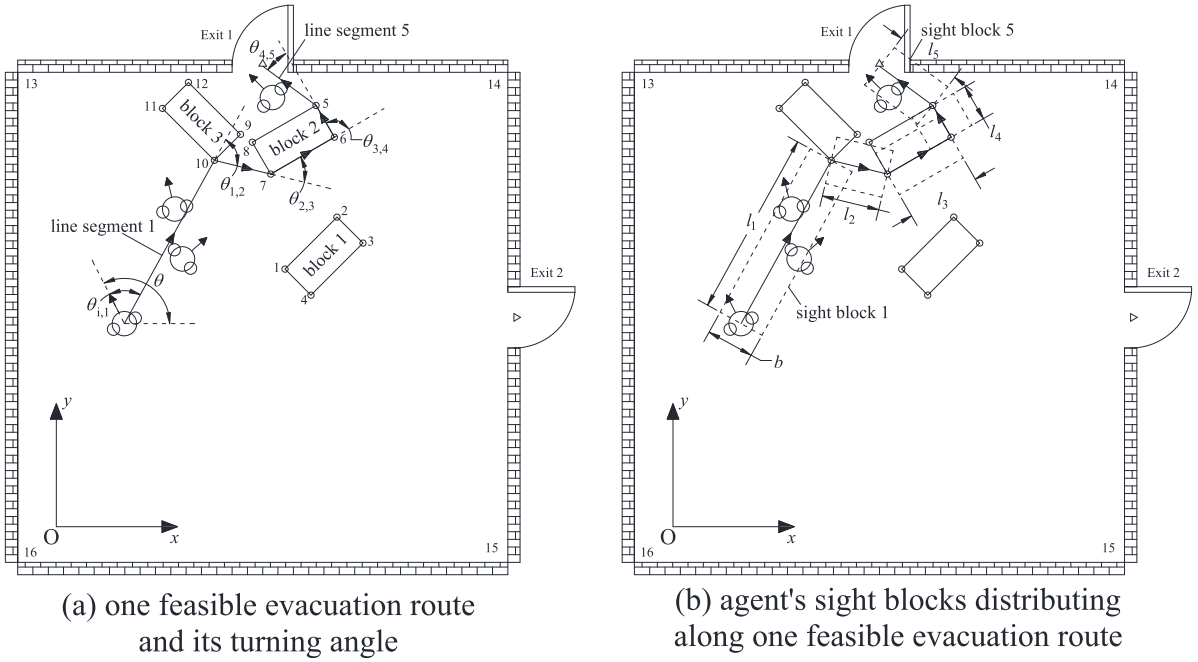


Fig. 10. Description of agent's DOFs, geometry, trial directions and positions.

feasible route 10-7-6-5-Exit 1 is selected for an agent, which is shown in Fig. 11, is used as an example. In this figure, important concepts and quantities, such as turning angle, traveling distance and sight blocks, are also illustrated. Their roles in the choice of final evacuation route from feasible ones are discussed in the following paragraphs.

Sight blocks are schematically shown on the right of Fig. 11 assuming that they can reach exit 1, which are represented by the dashed rectangles. Let  $l_v$  be the total sight length of an agent,  $n_e$  be the number of polyline representing the current feasible evacuation route, and  $l_i$  be the length of each line segment constituting the polyline ( $i = 1, 2, \dots, n_e$ ). The final number of sight blocks  $n_s$  should satisfy the following inequality:



**Fig. 11.** Turning angle, traveling distance and sight blocks associated with one feasible evacuation route.

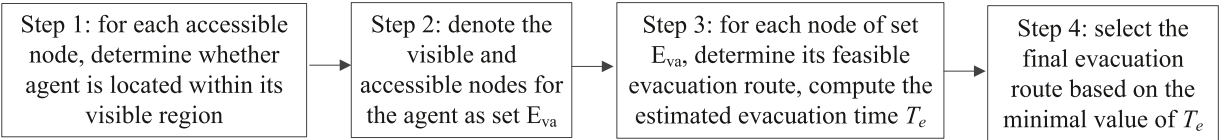


**Fig. 12.** Procedure to determine the final evacuation route.

$$\begin{cases} \sum_{i=1}^{n_s-1} l_i \geq l_v \text{ and } \sum_{i=1}^{n_s} l_i < l_v \text{ and } n_s \leq n_e, \text{ if } n_s \geq 2 \\ l_1 \leq l_v \text{ and } n_s \leq n_e, \text{ if } n_s = 1 \end{cases} \quad (1)$$

Clearly, from Eq. (1) if  $n_s \geq 2$  the length of the last sight block  $n_s$  should be  $l_v - \sum_{i=1}^{n_s} l_i$  and the first  $n_s - 1$  sight blocks have a length of  $l_i$  where  $i = 1, 2, \dots, n_s - 1$ . In this study the width of sight block is assumed as  $b = 4R_t$ . The total sight length  $l_v$  is dependent on agent's vision ability. To this end, a vision parameter  $\xi$  ranging from 0 to 1 is defined, with  $\xi = 0$  meaning agent's vision is completely impaired. The total sight length, agent's translational and angular velocity are assumed to depend on the vision parameter via the following equations:

$$\begin{cases} v_f = (0.5 + 0.5\xi)[v_f] \\ \omega = (0.5 + 0.5\xi)[\omega] \\ l_v = 8\xi \end{cases} \quad (2)$$

where  $[v_f]$  and  $[\omega]$  are the translational and angular velocity when agent's vision ability is full; it is assumed  $[v_f]$  conforms a uniform distribution from 1.0 to 1.2 m/s and  $[\omega]$  conforms a uniform distribution from  $\pi/2$  to  $2\pi/3$  rad/s unless otherwise stated, the value for angular velocity is adopted from [33].

With the sight blocks of an agent along one feasible evacuation route defined, agent can count how many other agents locate within the region covered by the sight blocks, denote this number as  $n_a$  in this study and  $n_a = 3$  in Fig. 11. With this number available, the turning angle  $\theta_t$  and traveling distance  $L_t$  can be computed as:

$$\theta_t = \theta_{i,1} + \sum_{j=1}^{n_e-1} \theta_{j,j+1} + n_a \times \frac{2\pi}{3}; L_t = \sum_{j=1}^{n_e} l_j + n_a \times 4R_t \quad (3)$$

where  $\theta_{i,1}$  is the smallest absolute angle that rotates agent's current facing direction to align with the first line segment of feasible evacuation route; similarly,  $\theta_{j,j+1}$  is the smallest absolute angle rotating the  $j$ th line segment to align with the  $j+1$ th one; the coefficients

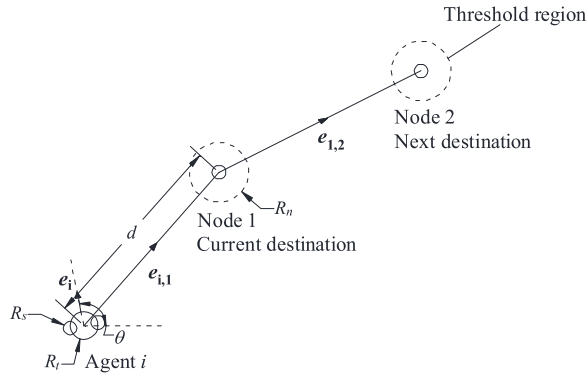


**Fig. 13.** Agent's movement along its final evauation route (only two accessible nodes are shown).

$\frac{2\pi}{3}$  and  $4R_t$  are used to account for the turning angle and traveling distance that an agent must take to avoid colliding with other agents. The estimated evacuation time  $T_e$  associated with this particular feasible evacuation route can be determined as:

$$T_e = \frac{\theta_t}{\omega} + \frac{L_t}{v_f} \quad (4)$$

Given agent's current position, which is represented by its coordinate  $[x,y]$ , the choice of final evacuation route can be determined via the procedure in Fig. 12. It should be noted that in Step 3, even for a single node of set  $E_{va}$ , there may be multiple feasible evacuation routes (e.g. there are two feasible evacuation routes for node 4 in Fig. 9(a)). And the requirement that the tree structure should include all accessible nodes guarantees there is at least one feasible evacuation route corresponding to any node of set  $E_{va}$ .

During agent-based simulation, it is not realistic to perform the above procedure to determine the final evacuation route for all agents at every time step. This is because for a large number of agents and complex room configuration, the tree structure of feasible evacuation routes is extremely large. Consequently performing Step 3 in Fig. 12 becomes very inefficient. To overcome this shortcoming, in this study each agent searches for its own final evacuation route at the beginning of the simulation, and it will perform the searching procedure in Fig. 12 only if one of the following conditions are satisfied: (1) the number of agents in the sight blocks of current agent (i.e.  $n_a$ ) exceeds a threshold number; (2) the agent is stuck. In this paper, this threshold number is fifteen unless otherwise stated. One binary index  $I_s$  is used to indicate whether an agent is stuck or not, with  $I_s = 1$  meaning agent is stuck. The agent is deemed stuck if the following condition is satisfied:

$$\sqrt{(x(t + \Delta t) - x(t))^2 + (y(t + \Delta t) - y(t))^2} \leq 0.5R_t \quad (5)$$

where  $t$  is the current time,  $\Delta t = 0.5s$  is an incremental time (not the time increment used for agent-based simulation),  $x$  and  $y$  are the agent's horizontal and vertical coordinate. Eq. (5) implies that an agent is deemed stuck if its position does not change to a certain extent given a period of time.

### 3.2. Attractive potential

The attractive potential  $P_i$  reflects agent's desire to achieve a certain goal. In the context of room evacuation, it can be interpreted as an agent tries to reach all accessible nodes along the final evacuation route in a sequential order. Because of this feature, the attractive potential is reformulated.

An example to illustrate the calculation of attractive potential is shown in Fig. 13 in which only two accessible nodes are shown along the evacuation route for simplicity. After an agent selects its final evacuation route, it intends to move along this polyline until the exit is reached. During the movement, agent tries to reach the first accessible node before moving to the second one. Therefore, it is important for the agent to identify its current destination and next destination during evacuation. Recall that the accessible node is actually one vertex of a block and agent also has a finite body size, therefore at any time the agent cannot overlap with the accessible node. To resolve this paradox, a threshold region, which is represented by a dashed circle around an accessible node in Fig. 13, is introduced. Agent locating inside this threshold region is deemed to have reached this accessible node, consequently the agent must update its current and next destination. In this study, the radius of threshold region  $R_n = 2R_t$ . In Fig. 13 since agent  $i$  is currently located outside threshold region of node 1, its current and next destination are node 1 and 2, respectively. If agent  $i$  is locating inside threshold region of node 1, its current destination becomes node 2 and next destination is node 3 (not shown in Fig. 13). When the exit is selected as the current destination, there is difficulty applying the concept of next destination since it does not exist. In this case, an imaginary node is added to the final evacuation route so agent can pass through exit (hence complete evacuation). The coordinate of this imaginary node is dependent on the exit. The coordinate of this imaginary node for exit 1 in Fig. 1 is assumed as [4,12], while it is [12,4] for that associated with exit 2.

With node 1 and node 2 being agent's current and next destination, the attractive potential for an agent can be formulated

separately given index  $I_s = 0$  or  $I_s = 1$ :

$$\text{for the case } I_s = 0 : P_i = c_1(d' - d) + c_2 \mathbf{e}_i' \cdot \mathbf{e}_{obj} \quad (6)$$

$$\text{for the case } I_s = 1 : \begin{cases} P_i = c_1(d' - d) + c_2 \mathbf{e}_i' \cdot \mathbf{e}_{obj}, & \text{if } d > d' \\ P_i = c_1'(d - d') + c_2 \mathbf{e}_i' \cdot \mathbf{e}_{obj}, & \text{if } d \leq d' \end{cases} \quad (7)$$

where  $c_1 = 600$ ,  $c_1' = 400$  and  $c_2 = -200$ ;  $d$  is the distance from agent's current position to its current destination;  $d'$  is the distance from agent's trial position to its current destination;  $\mathbf{e}_i'$  is agent's trial rotation vector associated with its trial direction, see Fig. 10(c) and (d) for details of trial directions and positions;  $\mathbf{e}_{obj}$  is the objective directional vector for an agent and  $\bullet$  is the dot product between two vectors. The objective directional vector is computed via:

$$\mathbf{e}_{obj} = \dot{\mathbf{e}}_{obj} / \| \dot{\mathbf{e}}_{obj} \|; \dot{\mathbf{e}}_{obj} = \left( 1 - \frac{2}{3} \exp(-d') \right) \mathbf{e}_{i,1} + \frac{2}{3} \exp(-d') \mathbf{e}_{i,2} \quad (8)$$

in which  $\mathbf{e}_{i,1}$  is the directional vector from agent to its current destination, and  $\mathbf{e}_{i,2}$  is the directional vector from its current destination to the next one, as shown in Fig. 13;  $\| \cdot \|$  denotes the Euclidean length of a vector. Note that the objective directional vector  $\mathbf{e}_{obj}$  is formulated as a weighted average between two directional vectors  $\mathbf{e}_{i,1}$  and  $\mathbf{e}_{i,2}$ . The weighting coefficient depends on the distance from agent's trial position to its current destination. As the agent approaches towards its current destination, the weighting coefficient of directional vector  $\mathbf{e}_{i,2}$  increases and the other weighting coefficient decreases, thus it gradually adjusts agent's rotational behavior.

It is useful to examine Eqs. (6) and (7) to gain insights into its effect on agent's behavior. Since the second term related to the rotational behavior is identical in both equations, only agent's translational behavior is affected by the index  $I_s$ . For the case  $I_s = 0$ , which means agent is not stuck, a positive value of  $c_1$  makes agent to choose the trial position such that  $d'$  is less than  $d$ , this usually means moving forward or sideways for an agent. For the case  $I_s = 1$  in which agent is stuck, the attractive potential explicitly considers two scenarios:  $d \geq d'$  and  $d < d'$ . Also note that  $c_1'$  is a positive but smaller constant than  $c_1$ . This fact suggests that any trial position, except the one agent currently locates, reduces its potential  $P_i$ . The rationale behind this approach is that when agent is stuck it attempts to resolve the current situation by moving to all available trial positions regardless of its direction. To encourage this behavior and reflect agent's preference to moving forward,  $c_1'$  is selected as a positive but smaller value than  $c_1$ . It is observed this approach can effectively resolve the situation in which multiple agents get stuck.

### 3.3. Repulsive potential and other issues with agent-based simulation

The repulsive potential includes two parts: the first part represents the interaction between the agent being considered and other agents, which is denoted as  $P_{ij}$ ; the second part reflects the interaction between the agent and its surrounding built environment, which is denoted as  $P_{iw}$ . In this study, the built environment specifically refers to the walls and obstacles in the room. The mathematical formulations of  $P_{ij}$  and  $P_{iw}$  are identical to those proposed in [38] with the following minor modifications:

- (1) When computing repulsive potential  $P_{ij}$ , the other agent  $j$  is not considered if its distance to agent  $i$  is larger than an influence distance  $d_{inf}$ . This influence distance is again dependent on the vision parameter  $\xi$  via:

$$d_{inf} = 3R_t + (3 - 3R_t)\xi \quad (9)$$

Note in Eq (9) even if agent's vision is fully impaired, the influence distance is still a finite value ( $3R_t$  in this study). This is not unreasonable because agent can still feel its neighboring region by hand even it cannot see anything.

- (2) The parameters,  $R_x$  and  $R_y$  shown in Fig. 10(b), to define the physical boundary of an agent due to physical and psychological reasons (represented by an elliptic shape), are assumed as:  $R_x = R_y = R_b$ , considering agent is willing to sacrifice its own space for the sake of global mobility.
- (3) An obstacle can be considered as an assembly of four walls, therefore the equations developed for walls in [38] are directly applicable for an obstacle. However, it is assumed that an obstacle only affects agent's translational behavior.

There are several issues with agent-based simulation that are not mentioned here (e.g. updating rule), they have been discussed in detail in [38]. The time step for agent-based simulation in this paper is selected as 0.01 s for the simulations in the next section.

## 4. Simulation results

This section aims to evaluate and validate the proposed agent-based model with turning behavior for room evacuation in the presence of obstacles. For this purpose, two simulations are performed and results are compared with published experiments. The first example is pedestrian evacuation in a room with an obstacle placed near the exit [39]. The second example is simulating evacuation process in a classroom with multiple obstacles [40].

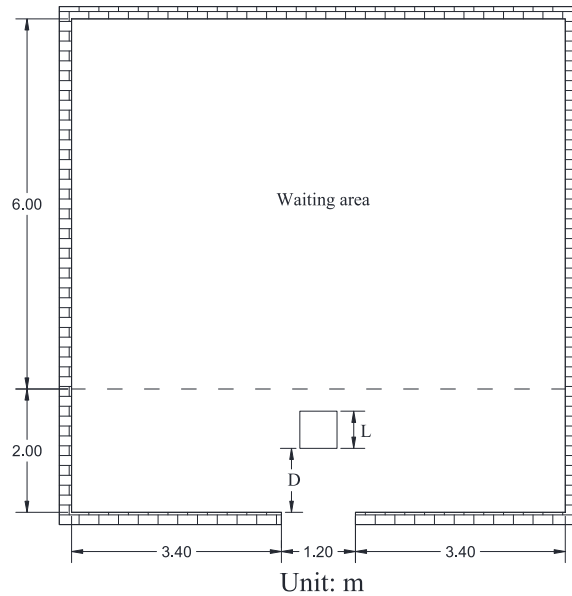


**Fig. 14.** Room evacuation with an obstacle in front of an exit.

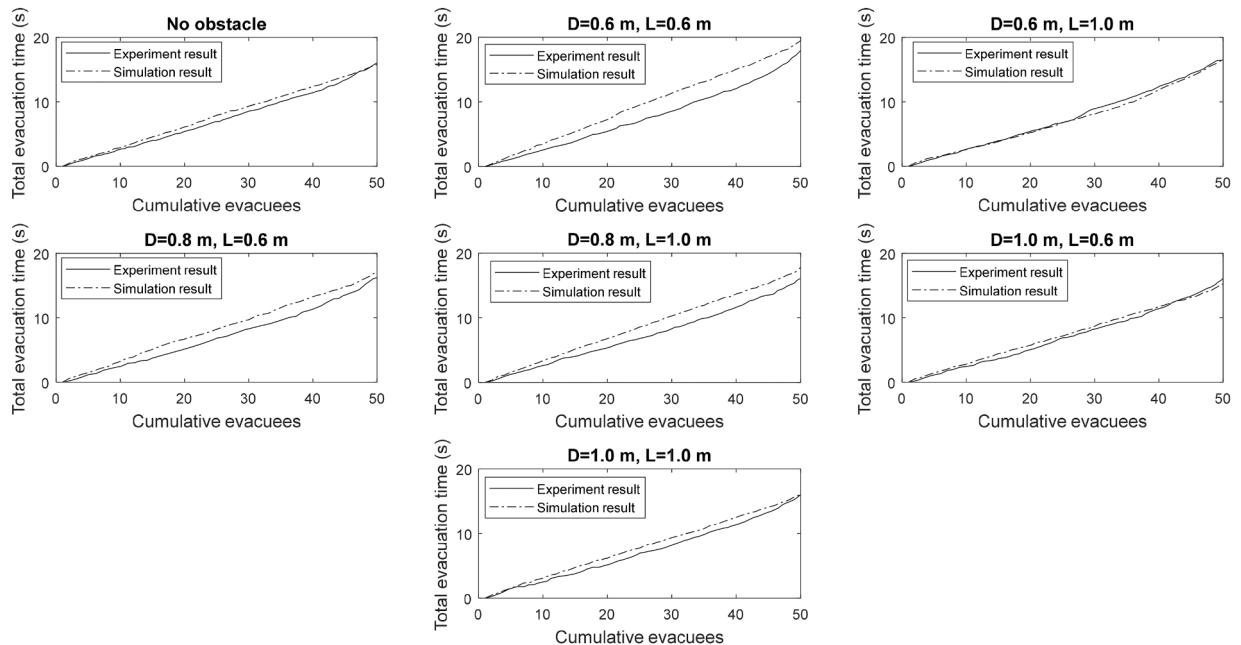


**Fig. 15.** Comparison of total evacuation time with experimental data.

#### 4.1. Room evacuation with an obstacle near exit

An experimental campaign is performed by Shi et al. [39]. In the experiment, fifty college students were asked to leave the room with an obstacle placed near the exit. The room has a size of 8 m by 8 m with an exit located on the middle of the bottom wall (referred to as middle exit in [39]). This exit has a length of 1.2 m. The room configuration is shown in Fig. 14. An obstacle with a square shape is placed near the exit. The dimensions of the obstacle and its clear distance to the exit are illustrated in Fig. 14. In this study,  $L = 0.6 \text{ m}$  and  $1.0 \text{ m}$ , and  $D = 0.6, 0.8$  and  $1.0 \text{ m}$ , which are consistent with experimental setup in [39]. Note that in real experiment the obstacle is a circular shape, but a square shape is used in the agent-based simulation instead for simplicity.

Fifty agents with random initial location and rotation are distributed within the waiting area in Fig. 14. The translational velocity of an agent [ $v_f$ ] is assumed to conform a uniform distribution ranging from 1.08 to 1.44 m/s, as is reported in [39]. The rotational velocity

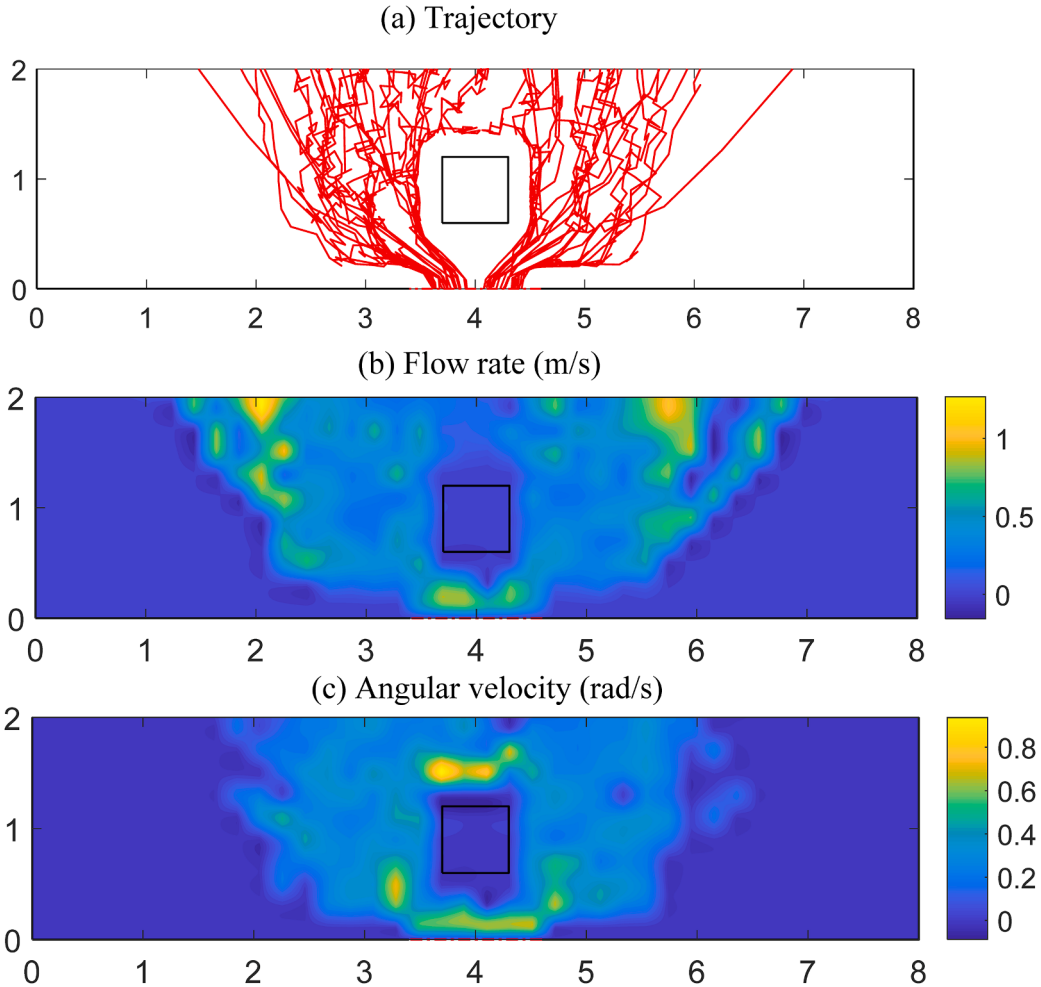


**Fig. 16.** Pedestrian trajectory, flow rate and angular velocity distribution with  $D = 0.6$  m and  $L = 0.6$  m in one agent-based simulation.

$[\omega]$  remains unchanged. The vision parameter  $\xi = 1$  is used for the numerical simulation. A parameter termed as total evacuation time is used for a quantitative comparison with experimental results. Total evacuation time is defined as the evacuation time for agent  $j$  ( $j > 1$ ) minus the first agent reaching the exit. For each combination of clear distance  $D$  and square size  $L$ , the agent-based simulation is repeated five times and average result is reported.

The comparison of total evacuation time with experimental results is presented in Fig. 15. It is observed that the agent-based model prediction is in a reasonable agreement with the experiment considering the complexity in the pedestrian behavior and its interaction with obstacle. The minimal and maximum total evacuation time predicted by the agent-based model is 15.3 s and 19.5 s, respectively. But the experimental results indicate they are roughly 16 s and 18 s. From Fig. 15, it is observed relatively large error occurs for the cases where  $D = 0.6$  m  $L = 0.6$  m,  $D = 0.8$  m  $L = 0.6$  m and  $D = 0.8$  m  $L = 1.0$  m. Besides the reason indicated above, it may also be attributed to the lack of statistics since numerical result is only averaged over five simulations. It is also observed that the presence of an obstacle near the exit may not necessarily increase the total evacuation time compared to the case of no obstacle: a phenomenon that has been reported in some studies (e.g. Frank and Dorso [18]). The trajectory of each agent, and their velocity distribution given  $D = 0.6$  m and  $L = 0.6$  m in one simulation are presented in Fig. 16. It can be seen that agent is translating and rotating in the evacuation process. The largest angular velocity occurs at two places: in front of the obstacle and the exit. These turning behavior is related to Eq. (8) in which agent adjusts its objective directional vector as it approaches (for the obstacle case) or changes (for the exit case) its current destination.

#### 4.2. Classroom evacuation

The second example to evaluate the performance of the proposed agent-based model is a simulation of classroom evacuation in which multiple obstacles are present. The classroom and obstacles inside it are shown in Fig. 17. The experimental setup, procedure, as well as results are presented in detail by Guo et al. [40]. In summary, thirty students are instructed to leave the classroom with

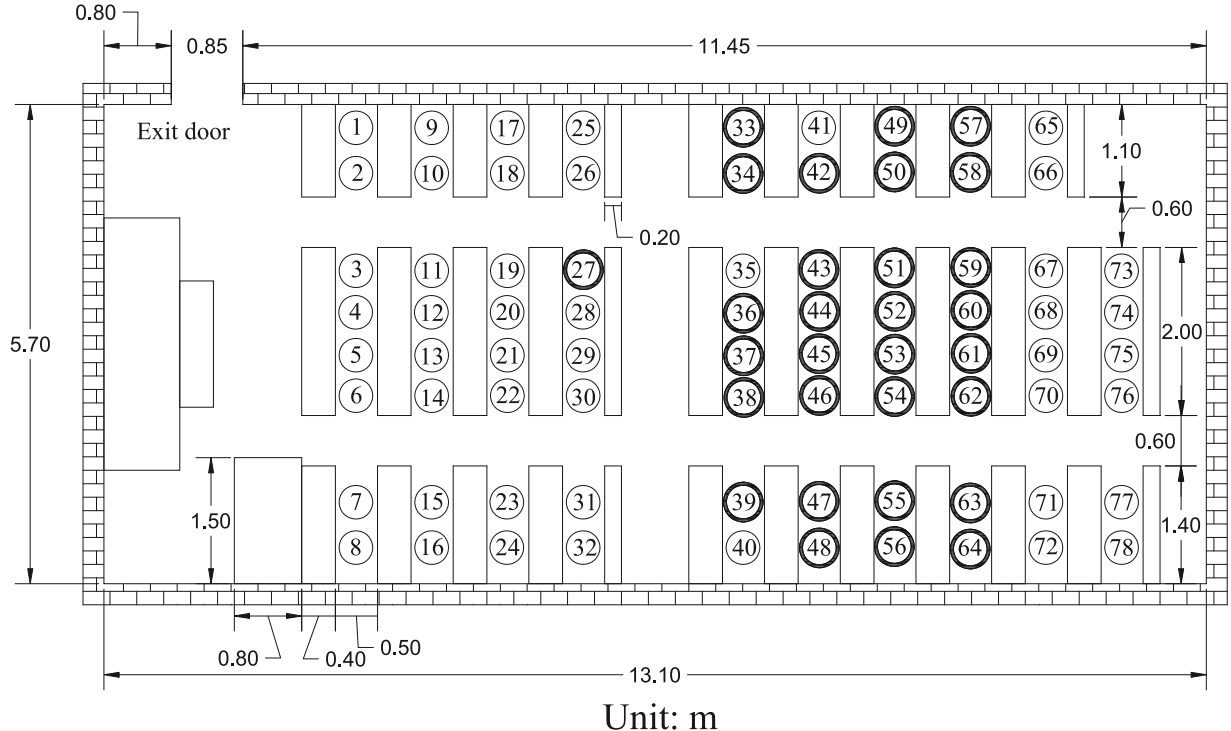


**Fig. 17.** Schematics of classroom evacuation (bold circles indicate experiment 1 setup).

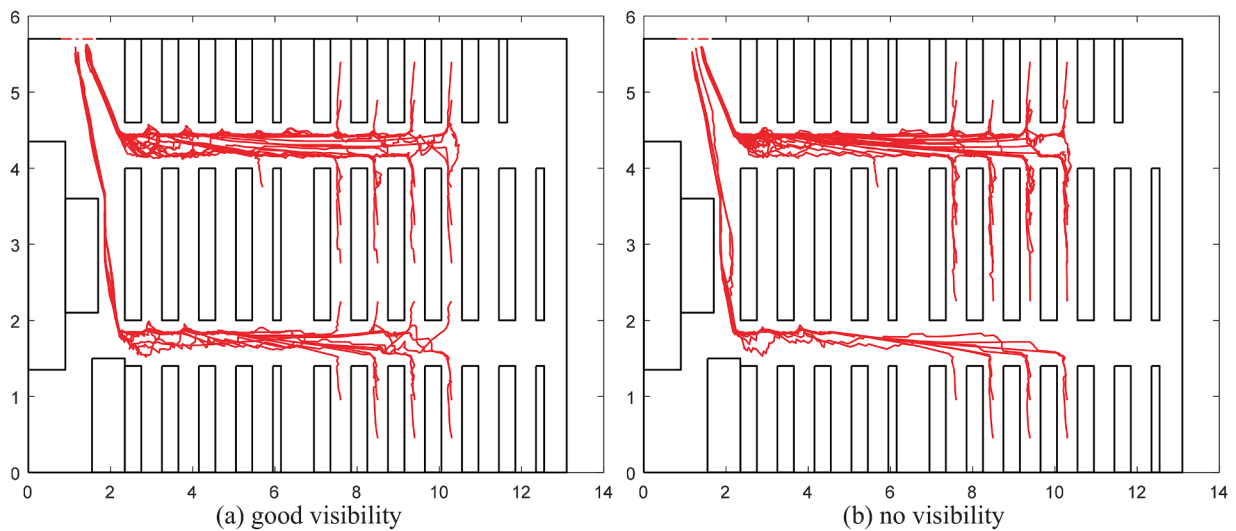


**Fig. 18.** Movement trajectory under different visibility conditions in experiment 1.

specified locations. The location number is also illustrated in Fig. 17 as the number in each circle. There are six experiments conducted in [40], each experiment is performed under the good visibility and no visibility condition. Here, no visibility means that each student wears an eye-patch so he/she cannot see things during experiment, good visibility means the opposite. The evacuation time for every student to reach the exit within each experiment is also recorded.

The developed agent-based model is used to reproduce this experiment using default parameters. To reflect different visibility conditions, the vision parameter  $\xi$  is set to 0 and 1 for no visibility and good visibility condition, respectively. Each agent's initial rotation is assumed to be  $\pi$  rad (i.e. facing left) and its initial location is based on the real experimental setup in [40]. Again, for each experiment with both visibility conditions, the agent-based simulation is repeated five times and average result is presented.

In experiment 1, thirty students initially located where the bold circle indicates in Fig. 17 are asked to leave the classroom. This

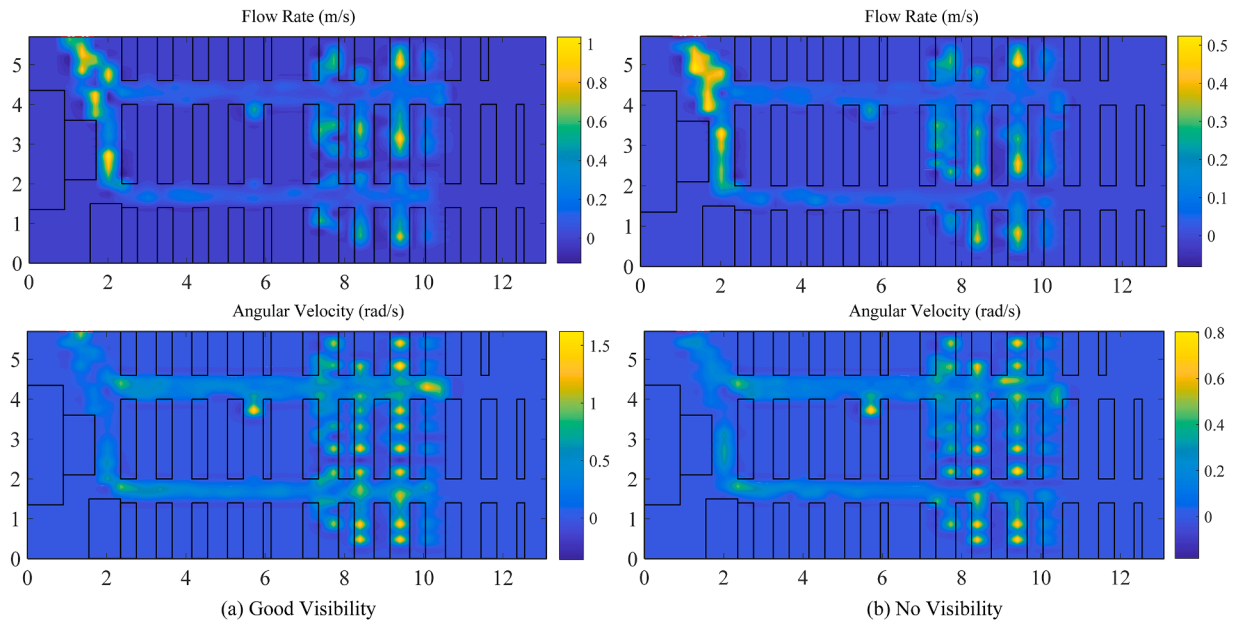


**Fig. 19.** Distribution of agent's velocity in experiment 1 under different visibility conditions.

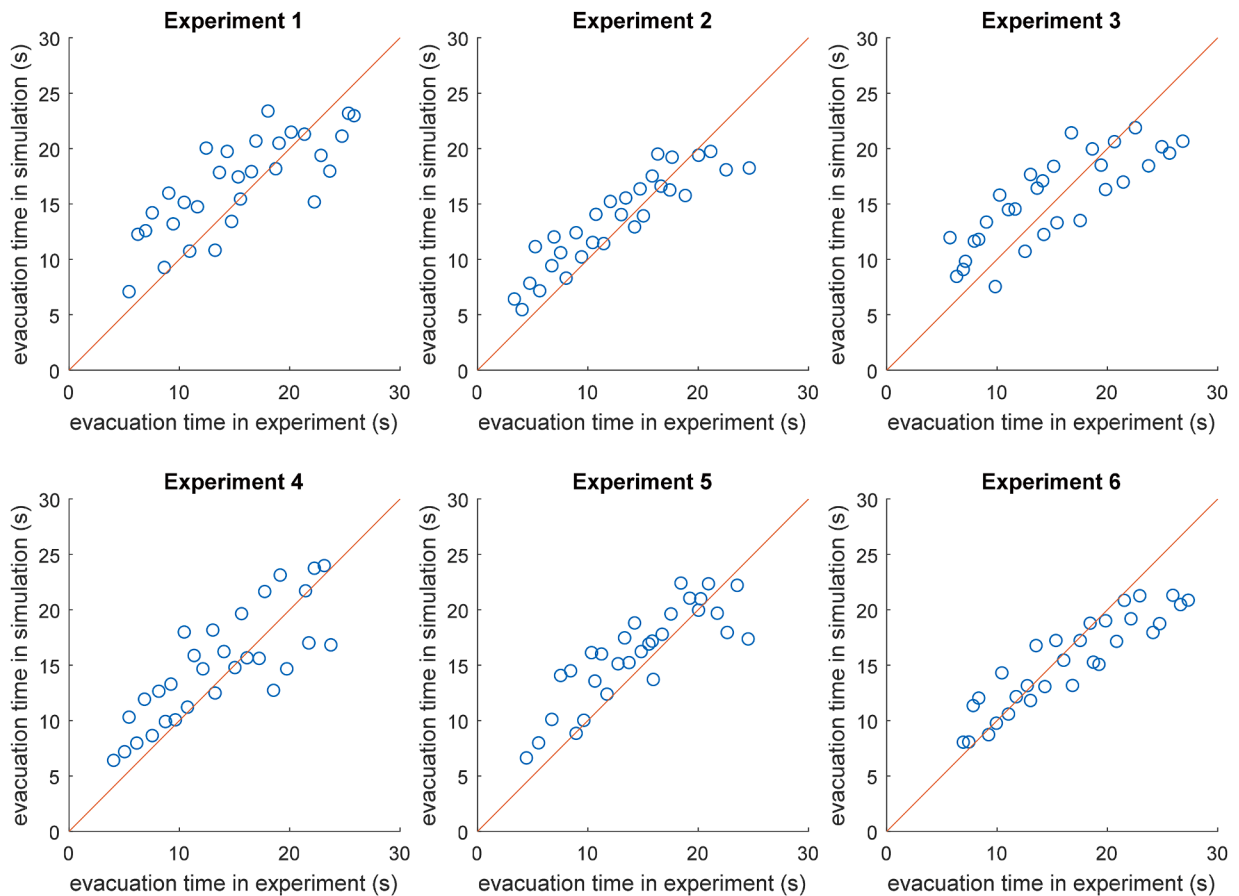


**Fig. 20.** Comparison of evacuation time for each agent under good visibility condition.

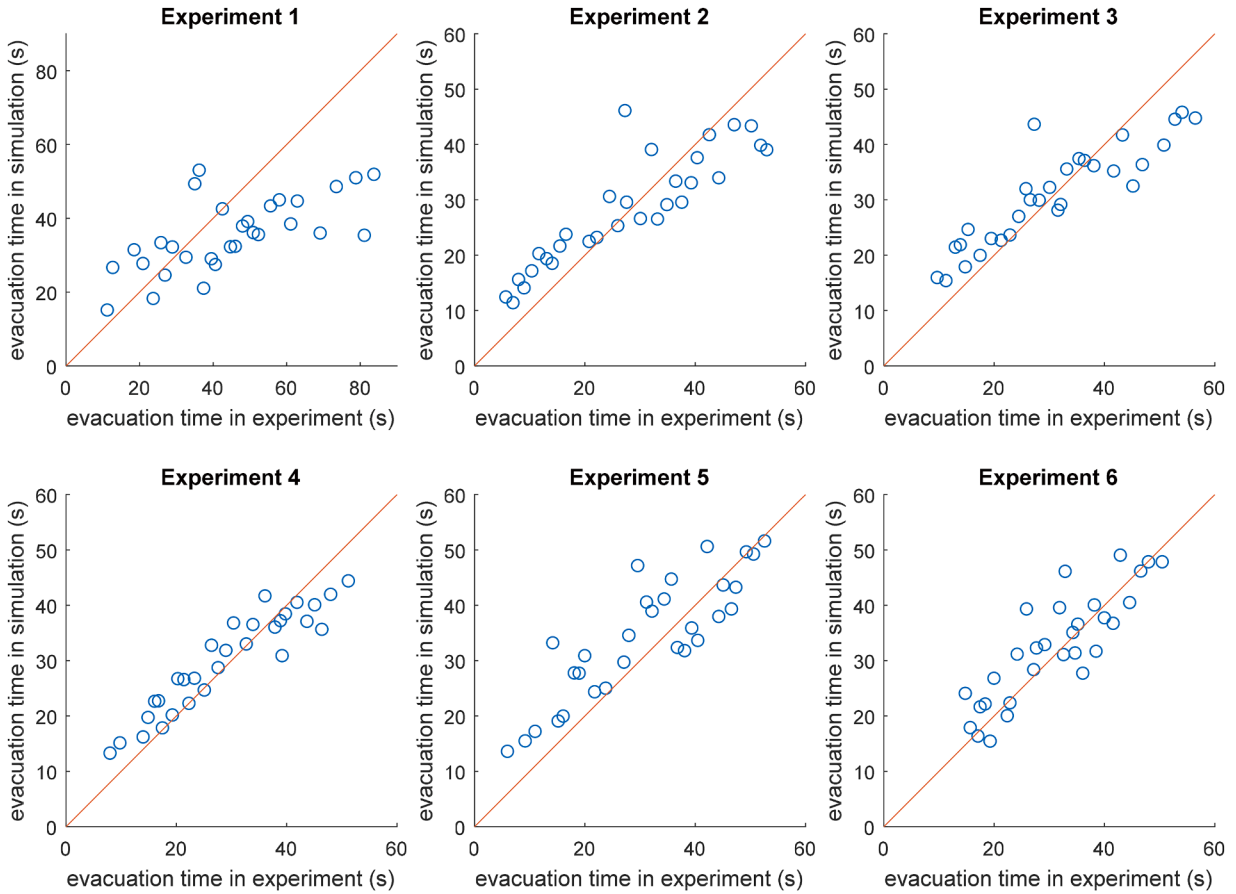


**Fig. 21.** Comparison of evacuation time for each agent under no visibility condition.

experiment is conducted under both good and no visibility conditions (i.e. with/without an eye-patch). The time each student evacuates from the classroom is recorded. Using this experiment as an example, the movement trajectories of each agent during classroom evacuation under different visibility conditions are presented in Fig. 18. It is observed that the vision parameter has a direct influence on the choice of final evacuation route for some agents. Under good visibility condition, agent initially located on circle number 38, 46, 54 and 62 moves downward. But these agents choose to move upward under no visibility condition. This is understandable because under good visibility condition agent can see other agents in its sight blocks and the estimated evacuation time increases accordingly. As a result, agent may select another evacuation route to save time. Under no visibility condition, agent will simply choose final evacuation route without considering the presence of other agents since they cannot be seen. This observation with agent-based simulation is also reported in the real experiment [40]. The translational and angular velocity distribution of agents in experiment 1 under different visibility conditions are presented in Fig. 19. The largest angular velocity happens at agent's initial position. This is understandable since each agent's initial rotation is  $\pi$  rad, which does not align with direction of evacuation route. The other location where angular velocity is relatively large occurs at the first column of obstacles (i.e. at horizontal coordinate around 2.5 m). This is the place where agent adjusts its facing direction to head for the exit. Note that the magnitudes of both velocities under good visibility condition are almost twice as large as that under no visibility condition, which is a result directly from Eq. (2). Also, it can be seen that the angular velocity is almost uniformly distributed along each agent's evacuation route. This is due to Eq. (8) which gradually adjusts agent's direction as agent moves along it.

Evacuation time of each agent in every experiment under both visibility conditions is compared with experimental data, as shown in Figs. 20 and 21. A line  $y = x$  is also included in these two figures for a better comparison. The closer each circle locates with respect to the line, the better the simulation result compares with experiment. It can be observed that the agent-based simulation results agree reasonably well with the experimental ones. The largest deviation from experimental result comes from experiment 1 under no visibility condition: the simulation predicts it needs 53 s for all agents to leave classroom, while the experiment record indicates 83.9 s is required, which may be an experimental anomaly. Based on the simulation results presented in these two sections, it is concluded the proposed agent-based model can qualitatively and quantitatively be used for room evacuation in the presence of multiple obstacles.

## 5. Conclusion

This paper presents an agent-based model for the room evacuation in the presence of multiple obstacles. Unlike previous studies on this topic which usually ignore the rotational behavior of pedestrian, the proposed agent-based model aims to take this behavior into consideration. To achieve this goal, this study extends a previously developed agent-based model for staircase evacuation to room evacuation. In reality, there are always multiple non-structural components in a room that may affect the pedestrian dynamics during evacuation. Therefore a careful consideration of the presence of multiple randomly located obstacles is essential for the successful application of the agent-based model. Based on the framework of agent-based model with rotational behavior, the following improvements are made considering the features of room evacuation:

- (1) A methodology to construct the visible region for a node of an obstacle or an exit is presented. The visible region is defined as a polygon area within which agent can see a node or an exit without any obstruction. It serves as the basis for the development of feasible evacuation routes and the choice of final evacuation route;
- (2) The concepts of accessible nodes, inaccessible nodes, and obstructed lines are introduced. Based on these concepts and visible region, a greedy method to generate the feasible evacuation routes for a given exit is presented;
- (3) A deterministic approach based on estimated evacuation time to select the final evacuation route from feasible ones is described. The estimated evacuation time takes traveling distance, turning angle, as well as number of agents along the evacuation route into account, which is a comprehensive evaluation;
- (4) The attractive potential, which represents agent's desire to achieve a certain goal, is reformulated accounting for agent's movement along its evacuation route. The repulsive potential between an agent and an obstacle is also briefly discussed.

The proposed agent-based model with rotational behavior for room evacuation is subsequently used in various scenarios to evaluate and validate its effectiveness. The first example is the simulation of room evacuation with an obstacle placed near exit. The total evacuation time under different combinations of size of obstacle and its clear distance to the exit is compared with experimental data. It is shown that the agent-based model is in agreement with published experimental result. The second example is concerned with classroom evacuation with multiple obstacles. It is observed that agent's choice of final evacuation route is affected by its vision ability, a phenomenon which is also reported in the real experiment. In addition, a detailed comparison of evacuation time for every agent in each experiment under various visibility conditions is performed. Relatively good agreement with recorded experimental data can be observed. Based on the above numerical simulation results, it is concluded the proposed agent-based model with rotational behavior can be used for room evacuation in the presence of multiple obstacles under relatively low density scenario. In a high density scenario, competitive or herding behavior may occur, which is not considered in the present framework of agent-based modeling. Potential application of this agent-based model includes: optimal design of architectural layout that minimizes the evacuation time, and pedestrian evacuation of residential room with multiple non-structural components randomly distributed after natural hazards (e.g. fire or earthquake). It is expected the proposed agent-based model can give both qualitative and quantitative predictions of key parameters in the room evacuation, thus facilitating design, risk management and development of safety code related to buildings under various hazards.

## References

- [1] E. Ronchi, D. Nilsson, Fire evacuation in high-rise buildings: a review of human behaviour and modelling research, *Fire Sci. Rev.* 2 (7) (2013) 1–21, <https://doi.org/10.1186/2193-0414-2-7>.
- [2] D. Alexander, Behavior during earthquakes: a southern Italian example, *Int. J. Mass Emerg. Disast.* 8 (1) (1990) 5–29.
- [3] S.P. Hoogendoorn, P.H.L. Bovy, Pedestrian route-choice and activity scheduling theory and models, *Transp. Res. Part B* 38 (2004) 169–190, [https://doi.org/10.1016/S0191-2615\(03\)00007-9](https://doi.org/10.1016/S0191-2615(03)00007-9).
- [4] M. Asano, T. Iryo, M. Kuwahara, Microscopic pedestrian simulation model combined with a tactical model for route choice behavior, *Transp. Res. Part C* 18 (6) (2010) 842–855, <https://doi.org/10.1016/j.trc.2010.01.005>.
- [5] S.M. Lo, H.C. Huang, P. Wang, K.K. Yuen, A game theory based exit selection model for evacuation, *Fire Saf. J.* 41 (5) (2006) 364–369, <https://doi.org/10.1016/j.firesaf.2006.02.003>.
- [6] A. Varas, M.D. Cornejo, D. Mainemer, B. Toledo, J. Rogan, V. Munoz, J.A. Valdivia, Cellular automaton model for evacuation process with obstacles, *Phys. A* 382 (2007) 631–642, <https://doi.org/10.1016/j.physa.2007.04.006>.
- [7] H.J. Huang, R.Y. Guo, Static floor field and exit choice for pedestrian evacuation in rooms with internal obstacles and multiple exits, *Phys. Rev. E* 78 (2008), 021131, <https://doi.org/10.1103/PhysRevE.78.021131>.
- [8] R. Alizadeh, A dynamic cellular automaton model for evacuation process with obstacles, *Saf. Sci.* 49 (2011) 315–323, <https://doi.org/10.1016/j.ssci.2010.09.006>.
- [9] R.Y. Guo, H.J. Huang, Route choice in pedestrian evacuation: formulated using a potential field, *J. Stat. Mech. Theory Exp.* (2011) P04018, <https://doi.org/10.1088/1742-5468/2011/04/P04018>.
- [10] M. Haghani, M. Sarvi, Human exit choice in crowded built environments: investigating underlying behavioural differences between normal egress and emergency evacuations, *Fire Saf. J.* 85 (2016) 1–9, <https://doi.org/10.1016/j.firesaf.2016.07.003>.
- [11] R. Lovreglio, E. Ronchi, D. Nilsson, An evacuation decision model based on perceived risk, social influence and behavioural uncertainty, *Simul. Model. Pract. Theory* 66 (2016) 226–242, <https://doi.org/10.1016/j.simpat.2016.03.006>.
- [12] M. Choi, S. Chi, Optimal route selection model for fire evacuations based on hazard prediction data, *Simul. Model. Pract. Theory* 94 (2019) 321–333, <https://doi.org/10.1016/j.simpat.2019.04.002>.
- [13] A. Kirchner, A. Schadschneider, Simulation of evacuation process using a bionics-inspired cellular automaton model for pedestrian dynamics, *Phys. A* (2002) 260–276, [https://doi.org/10.1016/S0378-4371\(02\)00857-9](https://doi.org/10.1016/S0378-4371(02)00857-9).
- [14] W. Liao, A.U.K. Wagoum, N.W.F. Bode, Route choice in pedestrians: determinants for initial choices and revising decisions, *J. R. Soc. Interface* 14 (2017), 20160684, <https://doi.org/10.1098/rsif.2016.0684>.

- [15] M. Haghani, M. Sarvi, Z. Shahhoseini, Evacuation behaviour of crowds under high and low levels of urgency: experiments of reaction time, exit choice and exit-choice adaptation, *Saf. Sci.* 126 (2020), 104679, <https://doi.org/10.1016/j.ssci.2020.104679>.
- [16] H. Li, J. Zhang, L. Xia, W. Song, N.W.F. Bode, Comparing the route-choice behavior of pedestrians around obstacles in a virtual experiment and a field study, *Transp. Res. Part C* 107 (2019) 120–136, <https://doi.org/10.1016/j.trc.2019.08.012>.
- [17] D. Helbing, P. Molnar, Social force model for pedestrian dynamics, *Phys. Rev. E* 51 (5) (1995) 4282–4286, <https://doi.org/10.1103/PhysRevE.51.4282>.
- [18] G.A. Frank, C.O. Dorso, Room evacuation in the presence of an obstacle, *Phys. A* 390 (2011) 2135–2145, <https://doi.org/10.1016/j.physa.2011.01.015>.
- [19] X. Jia, H. Yue, X. Tian, H. Yin, Simulation of pedestrian flow with evading and surpassing behavior in a walking passageway, *Simulation* 93 (12) (2017) 1013–1035, <https://doi.org/10.1177/0037549717734633>.
- [20] W. Xie, E. Lee, T. Li, M. Shi, R. Cao, Y. Zhang, A study of group effects in pedestrian crowd evacuation: experiments, modelling and simulation, *Saf. Sci.* 133 (2021), 105029, <https://doi.org/10.1016/j.ssci.2020.105029>.
- [21] H. Zhang, H. Liu, X. Qin, B. Liu, Modified two-layer social force model for emergency earthquake evacuation, *Phys. A* 492 (2018) 1107–1119, <https://doi.org/10.1016/j.physa.2017.11.041>.
- [22] K. Zhu, Y. Yang, Q. Shi, Study on evacuation of pedestrians from a room with multi-obstacles considering the effect of aisles, *Simul. Modell. Pract. Theory* 69 (2016) 31–42, <https://doi.org/10.1016/j.simpat.2016.09.002>.
- [23] W. Yuan, K.H. Tan, A novel algorithm of simulating multi-velocity evacuation based on cellular automata modeling and tenability condition, *Phys. A* 379 (1) (2007) 250–262, <https://doi.org/10.1016/j.physa.2006.12.044>.
- [24] L.A. Pereira, D. Burgarelli, L.H. Duczmal, F.R.B. Cruz, Emergency evacuation models based on cellular automata with route changes and group fields, *Phys. A* 473 (2017) 97–110, <https://doi.org/10.1016/j.physa.2017.01.048>.
- [25] L. Lu, C.Y. Chan, J. Wang, W. Wang, A study of pedestrian group behaviors in crowd evacuation based on an extended floor field cellular automaton model, *Transp. Res. Part C* 81 (2017) 317–329, <https://doi.org/10.1016/j.trc.2016.08.018>.
- [26] N. Chooramun, P.J. Lawrence, E.R. Galea, An agent based evacuation model utilising hybrid space discretisation, *Saf. Sci.* 50 (2012) 1685–1694, <https://doi.org/10.1016/j.ssci.2011.12.022>.
- [27] H. Kim, S. Han, Crowd evacuation simulation using active route choice model based on human characteristics, *Simul. Modell. Pract. Theory* 87 (2018) 369–378, <https://doi.org/10.1016/j.simpat.2018.07.014>.
- [28] V. Ha, G. Lykotrafitis, Agent-based modeling of a multi-room multi-floor building emergency evacuation, *Phys. A* 391 (2012) 2740–2751, <https://doi.org/10.1016/j.physa.2011.12.034>.
- [29] A. Turner, A. Penn, Encoding natural movement as an agent-based system: an investigation into human pedestrian behaviour in the built environment, *Environ. Plan. B* 29 (4) (2002) 473–490, <https://doi.org/10.1068/b12850>.
- [30] I. Zuriguela, I. Echeverría, D. Mazaa, R.C. Hidalgoa, C. Martín-Gómez, Contact forces and dynamics of pedestrians evacuating a room: the column effect, *Saf. Sci.* 121 (2020) 394–402, <https://doi.org/10.1016/j.ssci.2019.09.014>.
- [31] A. Garcimartín, D. Maza, J.M. Pastor, D.R. Parisi, C. Martín-Gómez, I. Zuriguel, Redefining the role of obstacles in pedestrian evacuation, *New J. Phys.* 20 (2018), 123025, <https://doi.org/10.1088/1367-2630/aaf4ca>.
- [32] Y. Zhao, T. Lu, L. Fu, P. Wu, M. Li, Experimental verification of escape efficiency enhancement by the presence of obstacles, *Saf. Sci.* 122 (2020), 104517, <https://doi.org/10.1016/j.ssci.2019.104517>.
- [33] H. Yamamoto, D. Yanagisawa, C. Feliciani, K. Nishinari, Body-rotation behavior of pedestrians for collision avoidance in passing and cross flow, *Transp. Res. Part B* 122 (2019) 486–510, <https://doi.org/10.1016/j.trb.2019.03.008>.
- [34] C.J. Jin, R. Jiang, J.L. Yin, D. LY, D.W. Li, Simulating bi-directional pedestrian flow in a cellular automaton model considering the body-turning behavior, *Phys. A* 482 (2017) 666–681, <https://doi.org/10.1016/j.physa.2017.04.117>.
- [35] D. Miyagawa, G. Ichinose, Cellular automaton model with turning behavior in crowd evacuation, *Phys. A* 549 (2020), 124376, <https://doi.org/10.1016/j.physa.2020.124376>.
- [36] Z. Fu, Q. Jia, J. Chen, J. Ma, K. Han, L. Luo, A fine discrete field cellular automaton for pedestrian dynamics integrating pedestrian heterogeneity, anisotropy, and time dependent characteristics, *Transp. Res. Part C* 91 (2018) 37–61, <https://doi.org/10.1016/j.trc.2018.03.022>.
- [37] Z. Fu, X. Zhan, L. Luo, A. Schadschneider, J. Chen, Modeling fatigue of ascending stair evacuation with modified fine discrete floor field cellular automata, *Phys. Lett. A* 383 (2019) 1897–1906, <https://doi.org/10.1016/j.physleta.2019.03.030>.
- [38] Y. Bao, F.Z. Huo, An agent-based model for staircase evacuation considering agent's rotational behavior, *Phys. A* 572 (2021), 125923, <https://doi.org/10.1016/j.physa.2021.125923>.
- [39] X. Shi, Z. Ye, N. Shiwakoti, D. Tang, J. Lin, Examining effect of architectural adjustment on pedestrian crowd flow at bottleneck, *Phys. A* 522 (2019) 350–364, <https://doi.org/10.1016/j.physa.2019.01.086>.
- [40] R.Y. Guo, H.J. Huang, S.C. Wong, Route choice in pedestrian evacuation under conditions of good and zero visibility: experimental and simulation results, *Transp. Res. Part B* 46 (2012) 669–686, <https://doi.org/10.1016/j.trb.2012.01.002>.